



**Passive, non-pharmacological sweat collection and analysis using a skin-interfaced, soft microfluidic system with colorimetric biomarker assays relevant to kidney disorders**

Journal:	<i>Lab on a Chip</i>
Manuscript ID	LC-ART-01-2019-000103.R1
Article Type:	Paper
Date Submitted by the Author:	08-Mar-2019
Complete List of Authors:	Zhang, Yi; University of Missouri Columbia Archives, Guo, Hexia; Northwestern University Kim, Sung Bong; University of Illinois at Urbana-Champaign Wu, Yixin; Northwestern University Ostojich, Diana ; University of Illinois at Urbana-Champaign Park, Sook; Northwestern University Wang, Xueju ; University of Missouri System Li, Rui; Dalian University of Technology Bandodkar, Amay; University of California San Diego Sekine, Yurina; Nihon Genshiryoku Kenkyu Kaihatsu Kiko, Materials Sciences Research Center Weng, Zhengyan; University of Missouri System Choi, Jungil; Northwestern University Xu, Steve; Northwestern University Feinberg School of Medicine, Department of Dermatology Quaggin, Susan ; Northwestern University Ghaffari, Roozbeh; Northwestern University Rogers, John; Northwestern University



## Passive sweat collection and colorimetric analysis of biomarkers relevant to kidney disorders using a soft microfluidic system

Yi Zhang,<sup>a,b</sup> Hexia Guo,<sup>b</sup> Sung Bong Kim,<sup>c</sup> Yixin Wu,<sup>b</sup> Diana Ostojich,<sup>c</sup> Sook Hyeon Park,<sup>d</sup> Xueju Wang,<sup>e</sup> Zhengyan Weng,<sup>a</sup> Rui Li,<sup>f</sup> Amay J. Bandodkar,<sup>b</sup> Yurina Sekine,<sup>g</sup> Jungil Choi,<sup>h</sup> Shuai Xu,<sup>ij</sup> Susan Quaggin,<sup>d</sup> Roozbeh Ghaffari,<sup>i,k</sup> and John A. Rogers<sup>\*b,i</sup>

Received 00th January 20xx,  
Accepted 00th January 20xx

DOI: 10.1039/x0xx00000x

[www.rsc.org/](http://www.rsc.org/)

The rich range of biomarkers in sweat and the ability to collect sweat in a non-invasive manner create interest in the use of this biofluid for assessments of health and physiological status, with potential applications that range from sports and fitness to clinical medicine. This paper introduces two important advances in recently reported classes of soft, skin-interfaced microfluidic systems for sweat capture and analysis: (1) a simple, broadly applicable means for collection of sweat that bypasses requirements for physical/mental exertion or pharmacological stimulation and (2) a set of enzymatic chemistries and colorimetric readout approaches for determining the concentrations of creatinine and urea in sweat, throughout ranges that are physiologically relevant. The results allow for routine, non-pharmacological capture of sweat for patient populations, such as infants and the elderly, that cannot be expected to sweat through exercise, and they create potential opportunities in the use of sweat for kidney disease screening/monitoring. Studies on human subjects demonstrate these essential capabilities, with quantitative comparisons to standard methods. The results expand the range of options available in microfluidic sampling and sensing of sweat for disease diagnostics and health monitoring.

### Introduction

As a representative biofluid, sweat contains a wealth of biomarkers relevant to health status, from electrolytes and metal ions, to metabolites, amino acids, proteins, and hormones.<sup>1,2</sup> By comparison to blood and interstitial fluids, the ability to collect sweat non-invasively creates opportunities for use in routine diagnostics via wearable platforms, with potential applications ranging from sports physiology to clinical medicine.<sup>3</sup> As an example of the former, quantitative information on the loss of sodium and chloride through sweat can be used by athletes to guide proper management of electrolyte balance.<sup>4</sup> As an example of the latter, the concentration of chloride in sweat is the primary clinical standard indicator of cystic fibrosis in newborns and infants.<sup>5</sup> Recent research suggests additional possibilities for sweat-based diagnostics, including the use of concentrations of cortisol and glucose in sweat as indicators of stress/fatigue and diabetes, respectively.<sup>6-9</sup> In addition to sweat chemistry, the

volume and rate of sweat loss provide quantitative information on conditions such as hyper- and hypo-hidrosis.<sup>10</sup> Furthermore, the concentrations of biomarkers in sweat and the sweat rate are linked due to the intrinsic nature of the mechanisms of secretion and reabsorption.<sup>11-13</sup> For example, the concentrations of urea and creatinine increase with decreasing sweat rate, while the concentrations of sodium and chloride show opposite trends.<sup>14,15</sup> Measurements of rate are, as a result, essential for meaningful interpretation of sweat biochemistry.

Here, we present simple colorimetric schemes to assess the sweat rate and the concentrations of urea and creatinine, as two metabolic products in sweat that could provide indications relevant to kidney function. Healthy kidneys remove creatinine and urea from the blood via glomerular filtration,<sup>16</sup> a key aspect of renal function. The concentration of creatinine in serum can, therefore, provide an estimate of glomerular filtration rate (eGFR).<sup>17</sup> Blood urea nitrogen (BUN) yields information about eGFR and renal tubular function, because BUN is not only freely

<sup>a</sup> Department of Biomedical, Biological, and Chemical Engineering, University of Missouri, Columbia, MO 65211, USA

<sup>b</sup> Department of Materials Science and Engineering, Northwestern University, Evanston, IL 60208, USA. E-mail: jrogers@northwestern.edu

<sup>c</sup> Department of Materials Science and Engineering, and Frederick Seitz Materials Research Laboratory, University of Illinois at Urbana-Champaign, Urbana, IL 61801, USA

<sup>d</sup> Division of Nephrology and Hypertension, Feinberg Cardiovascular and Renal Research Institute, Feinberg School of Medicine, Northwestern University, Chicago, IL 60611

<sup>e</sup> Department of Mechanical and Aerospace Engineering, University of Missouri, Columbia, MO 65211, USA

<sup>f</sup> State Key Laboratory of Structural Analysis for Industrial Equipment, Department of Engineering Mechanics, and International Research Center for Computational Mechanics, Dalian University of Technology, Dalian 116024, China

<sup>g</sup> Materials Sciences Research Center, Japan Atomic Energy Agency, Tokai, Ibaraki, 319-1106, Japan

<sup>h</sup> School of Mechanical Engineering, Kookmin University, 77 Jeongneung-ro, Seongbuk-gu, Seoul 02707, Korea

<sup>i</sup> Center for Bio-Integrated Electronics, Simpson Querry Institute for BioNanotechnology, Northwestern University, Evanston, IL 60208, USA

<sup>j</sup> Department of Dermatology, Feinberg School of Medicine Center for Bio-Integrated Electronics, Northwestern University, Chicago, IL 60211, USA

<sup>k</sup> Department of Biomedical Engineering, Northwestern University, Evanston, IL 60208, USA

filtered through glomeruli, but it is also absorbed via renal tubular cells.<sup>18</sup> As a result, serum creatinine and BUN serve as the basis for tests of glomerular function.<sup>19</sup> Specifically, as kidneys fail, the efficiency of this process diminishes, and the concentrations of urea and creatinine in the blood both increase.<sup>20,21</sup> The current standard of care in screening for kidney dysfunction involves measurements in samples of blood and/or urine using laboratory techniques, such as liquid chromatography and nuclear magnetic resonance spectroscopy (NMR). Such testing procedures are, however, costly and they must be performed by trained personnel in laboratories or hospitals.

Due to diffusive equilibration processes, these changes in blood chemistry can lead to corresponding changes in the concentration of these species in sweat.<sup>22</sup> In particular, the levels of sweat creatinine and urea are higher in kidney patients than in healthy subjects.<sup>16,23</sup> Average urea concentrations in sweat range from ~5 to ~40 mM for healthy subjects.<sup>16,24</sup> The creatinine concentration in healthy males is ~0.03 mM.<sup>16</sup> As an additional parameter, the pH of sweat can be useful in characterizing various health conditions,<sup>25</sup> and it is an indicator of metabolic alkalosis.<sup>26</sup> Of particular relevance here is that sweat pH, which is often coupled to the concentration of sodium in sweat, can be used for monitoring for dehydration.<sup>25,27</sup> Low urine pH is an independent predictor of stage 3 chronic kidney diseases.<sup>28</sup>

Although the connections between chronic kidney disease and sweat parameters are not completely understood, there are reasons to believe that sweat pH, creatinine and urea concentrations will be important. A key challenge in establishing relationships between biomarkers in sweat and different stages of chronic kidney disease arises from difficulties in collecting sweat samples while simultaneously quantifying sweat rate and volume, and avoiding confounding effects associated with sweat evaporation or compensatory sweating.<sup>29</sup> Traditional techniques rely on extraction of sweat from absorbent pads or rigid tubular collection platforms followed by transfer into benchtop instruments for analysis. The accuracy of the procedures can be compromised by evaporation and/or contamination during sweat collection, storage and transfer, and they cannot be used outside of specialized facilities.<sup>1</sup>

Simple, non-invasive methods that enable sweat capture and analytics directly on sweat as it emerges from the skin are of interest in this context. Specifically, recent advances in wearable electronics, soft microfluidics, and electrochemical/colorimetric sensors provide attractive sets of capabilities.<sup>30-35</sup> These approaches retain, however, requirements for heavy exercise or for pharmacological stimulation to generate sufficient quantities of sweat for analysis.<sup>9,36-38</sup> The former limits applicability to patients who are physically fit and able to exercise. The latter demands the use of iontophoresis for transdermal delivery, and an associated collection of electronics and skin-electrode interfaces that can cause discomfort and inflammation.

This paper reports a set of results that addresses issues in both analysis and collection of sweat, with a focus on kidney

disease. The approach to collection exploits water-proof, skin-interfaced microfluidic systems to capture sweat released naturally, immediately after and especially during warm-water showering or bathing. Analysis relies on enzymatic chemistries and colorimetric readout schemes implemented within the device structures. We note that while these procedures offer attractive features relative to other options in sweat collection/analysis, they do not support continuous monitoring, as they require the subject to engage in certain activities. These technology platforms and procedures enable investigations of sweat creatinine and urea and their relationships to chronic kidney disease stages, as the first step toward the potential development of a testing approach that does not require blood.

## Results

### Soft epidermal microfluidic devices for capturing sweat

Sweat capture and manipulation occurs in a soft, epidermal microfluidic device that uses natural pressures associated with perspiration (~70 kPa) to induce filling (Fig. 1a),<sup>39</sup> based on materials and designs reported elsewhere.<sup>1,39</sup> The key functions of the devices described here include 1) analysis of the concentrations of creatinine and urea in sweat, as well as its pH and 2) evaluation of sweat rate and sweat loss (Fig. 1a). As sweat enters the device from inlet ports at the skin interface, it passes through microscale channels ( $\mu$ -channels) and collects into a series of microscale reservoirs ( $\mu$ -reservoirs) that fill in a sequential manner due to the use of a collection of capillary bursting valves.<sup>40</sup> Each  $\mu$ -reservoir contains a paper-based chemical assay or enzymes for colorimetric detection, as described subsequently. The sequential filling allows for evaluation of changes in sweat chemistry as a function of sweat loss. Serpentine-shaped  $\mu$ -channels that connect to a separate inlet port enable simultaneous measurements of sweat rate and total loss. Here, a water-soluble dye located at the inlet imparts color to the sweat as it enters the device, thereby facilitating visualization of the extent of filling.

An exploded view schematic illustration highlights various aspects of the multilayered structure of the system (Fig. 1b). An ultrathin, soft biomedical adhesive (1524; 3M, MN, USA; thickness: 60  $\mu$ m) with openings that define the sweat collection zones (~2.4 mm in radius for the analysis of creatinine and urea concentrations, and pH; ~1.5 mm in radius for the evaluation of rate and loss) at the inlet ports on the skin-interfaced side of the device establishes a route for sweat to enter and creates a water-tight seal and strong bond to the skin in other regions. The techniques of soft lithography yield a microfluidic layer of poly(dimethylsiloxane) (PDMS; ~550  $\mu$ m thick) that includes (1) a serpentine  $\mu$ -channel for measuring local sweat rate and loss and (2) three other  $\mu$ -channels that connect to three separate sets of connected, circular  $\mu$ -reservoirs configured for measurements of pH and of concentrations of creatinine and urea. Chemical assay components in each  $\mu$ -reservoir support colorimetric sensing of each of these species. A capping layer (PDMS; ~350  $\mu$ m thick) seals the entire system. A thin transparent polyester adhesive

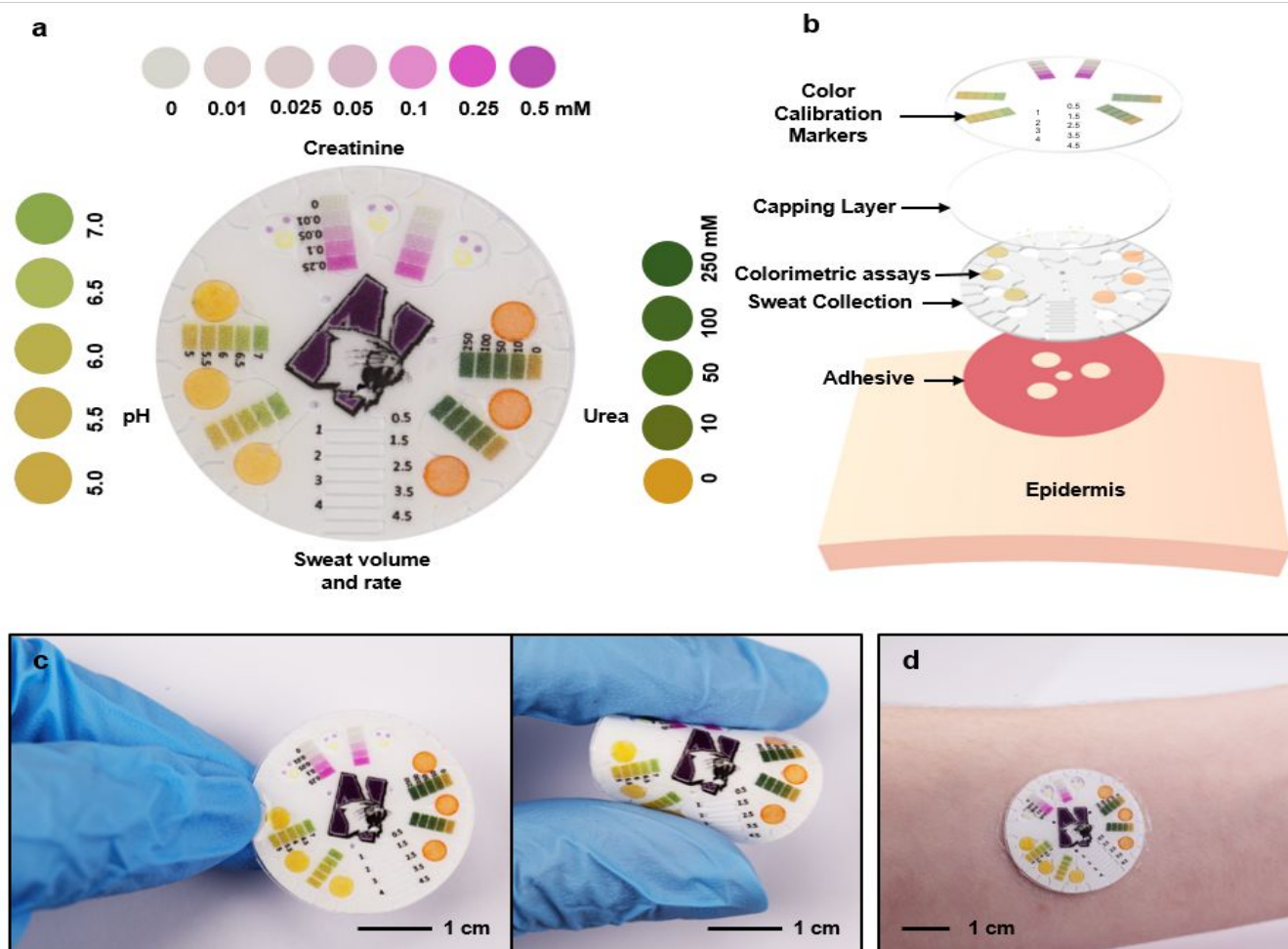


**Figure 1.** Overview, schematic illustration, and optical images of an epidermal microfluidic sweat sensor. (a) Overview of the functionality of the colorimetric detection scheme with insets at the right, left and top that illustrate the range of colors across a corresponding relevant range for sweat. (b) Exploded view illustration of the different layers and components of the system. (c) Image of a device in a flat (left) and bent (right) state. (d) Image of a device mounted on the forearm.

film (THERML film SELECT® 10852; FLEXcon, MA, USA; 25  $\mu\text{m}$  thick) with printed color reference markers bonds to this capping layer to aid the quantitative extraction of color information from digital images of the device. Fig. 1c shows an image of a representative device in a deformed state. The ability to bend freely allows the device to bind tightly to the skin in a non-invasive and non-irritating manner (Fig. 1d).

#### Quantitative colorimetric analysis

As described previously, creatinine and urea are important biomarkers of renal function. The concentration of creatinine in serum serves as a measure of the glomerular filtration rate (GFR) and provides a clinically accepted index of renal function.<sup>17</sup> Creatinine can be measured using the Jaffe method,<sup>41</sup> isotope dilution-liquid chromatography-mass spectrometry (IDLC-MS),<sup>42</sup> gas chromatography-mass spectrometry (GC-MS)<sup>43</sup> or capillary electrophoresis.<sup>44</sup> The scheme reported here relies on a colorimetric assay (Creatinine Assay Kit, MAK080, Sigma-Aldrich, MO) that is suitable for use with serum, plasma, urine, and other biological fluids. This assay involves a  $\text{H}_2\text{O}_2$ -responsive dye (4-aminophenazone) and a

sequence of reactions catalyzed by enzymes that include creatininase, creatinase, sarcosine oxidase, and peroxidase.<sup>45</sup> Although bilirubin is known to interfere with this assay, sweat is free of bilirubin.<sup>46</sup> Casting corresponding solutions of the enzymes and the probe with optimized formulations into the  $\mu$ -reservoirs and drying under vacuum creates active films for colorimetric sensing of creatinine concentrations relevant to sweat. Analysis involves quantitatively relating the decrease in the green level of RGB values extracted from images of a  $\mu$ -reservoir with increases in creatinine concentration, for a range between 0–500  $\mu\text{M}$  (Fig. 2a).

Most methods for measuring urea rely on LC-MS<sup>47</sup> and HPLC,<sup>48</sup> NMR,<sup>49</sup> or electrochemical techniques.<sup>50–52</sup> Commercially available urea colorimetric assay kits operate over a range of concentrations (0.01–0.1 mM) that is too low for evaluation of sweat. Healthy humans have urea concentrations between 0 and 50 mM; concentrations above 100 mM are suggestive of kidney dysfunction.<sup>16,23</sup> The colorimetric strategies introduced here address this full range via a scheme that colorimetrically evaluates increases in pH that result from the production of ammonium and hydroxyl ions ( $\text{OH}^-$ ) by urease

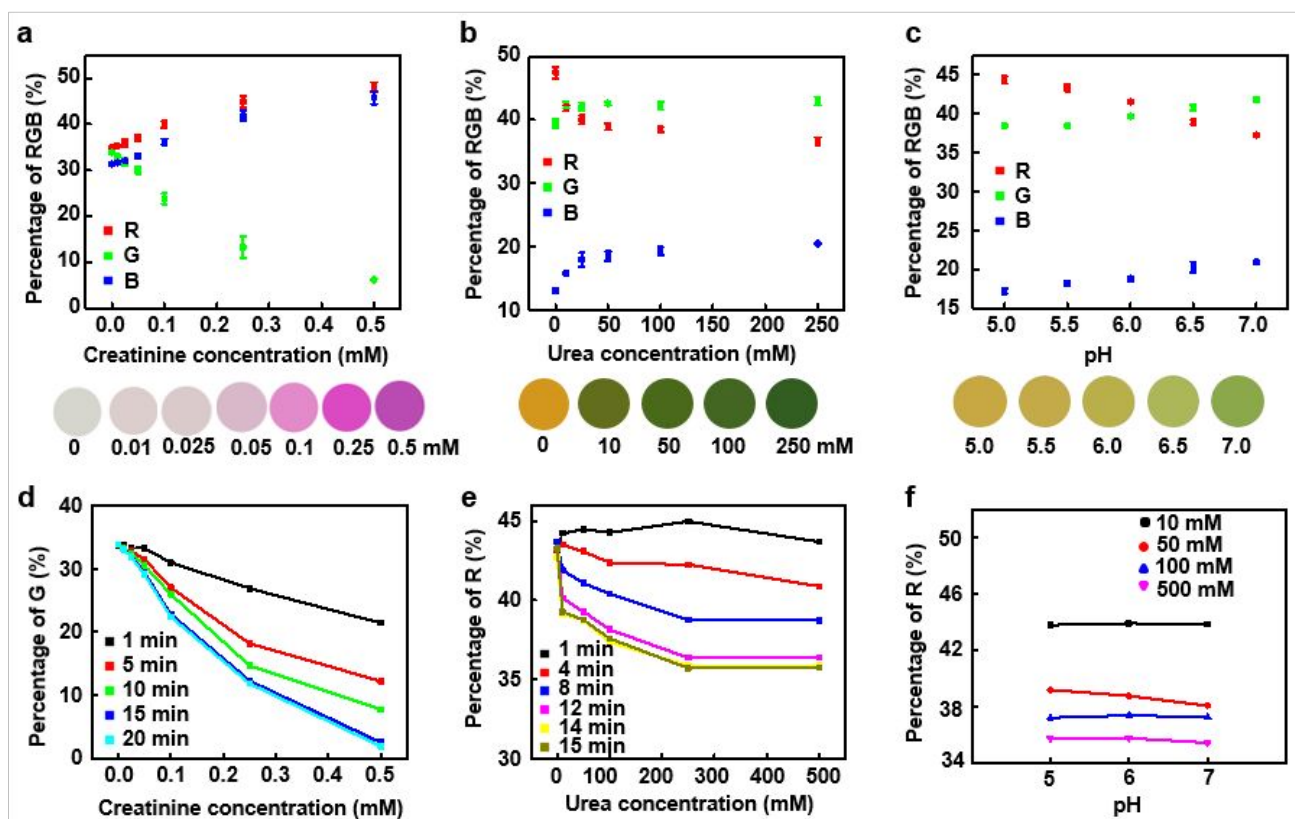


**Figure 2.** Quantitative colorimetric analysis of sweat creatinine, urea, and pH. Standard calibration curve between normalized percentage of red, green and blue levels from RGB analysis of the image and concentration of (a) creatinine, (b) urea and (c) pH. The normalized percentage of the change in green and red levels with time at various concentrations of (d) creatinine and (e) urea. (f) Plateau, normalized percentage of red level with pH at various sweat urea concentrations.

mediated hydrolysis of urea.<sup>53</sup> This catalytic effect of urease, immobilized in pH paper, raises the pH.<sup>54,55</sup> The resulting changes in the color of the pH paper correlate to the concentration of urea (Fig. 2b). Specifically, as the concentration of urea in sweat increases, the red level decreases with concentration from 10, 50, 100 to 250 mM, corresponding to pH values from 7.1, 8.4, 8.8, to 8.9. For concentrations above 100 mM, the value reaches a plateau, corresponding to a pH  $\sim$  8.9, due to the ammonia deactivation of urease.<sup>56</sup>

The evaluation of pH occurs separately using an indicator optimized for sensitivity across a range relevant to sweat (pH 5 to 7)<sup>57</sup> which includes dyes such as bromothymol blue, methyl red and phenolphthalein to yields colorimetric responses (Fig. 2c).

As shown in Figs. 2d-e, the RGB values extracted from digital images of these assays collected at 37 °C and under white light conditions gradually stabilize with time upon introduction of aqueous solutions of urea or creatinine at known concentrations until they reach a final state. For concentrations across ranges relevant to sweat at pH 6, the saturated, stabilized final state for both urea and creatinine assays occurs within 15 minutes at body temperature. The color response time of pH paper is less than one second.

The rate of hydrolysis of urea into ammonium and OH<sup>-</sup> can be influenced by the pH of sweat,<sup>58</sup> which typically lies between

5-7 due to the secretion of metabolic lactic acid.<sup>59</sup> Analyzing the percentage change in red level from RGB values collected as a function of time under physiologically relevant ranges of pH and various sweat urea concentrations suggests that pH influences the dynamics of color development. Specifically, changes in color cease after  $\sim$ 35, 15 and 14 min diminish for pH of 5, 6, and 7 respectively (Figs. S1a-c); the latter two values are similar possibly because as the pH approaches a neutral value, the differences in reaction rate are small. The sweat pH, however, does not significantly influence the final colors across various urea concentrations (Fig. 2f).

As mentioned previously, sweat rate affects the concentration of biomarkers in sweat. Specifically, the concentrations of urea and creatinine increase with decreasing sweat rate.<sup>14</sup> A decrease in the rate of sweating, for otherwise similar conditions, is an indicator for dehydration,<sup>60</sup> an important factor in kidney disorders.<sup>61</sup> Increasing water intake may have beneficial effects on renal function of patients with chronic kidney disease.<sup>61</sup> Measurements of sweat rate and loss are, therefore, important in the context of applications considered here. Options include capacitance hygrometry,<sup>62,63</sup> electrical impedance,<sup>11,13</sup> and, most recently, the kinetics of filling into microfluidic systems like those reported here.<sup>39</sup> For this third option, fluid delivered using external pumping apparatus mimics the process of sweating to allow for calibration (Fig. S2). A green dye located in a  $\mu$ -reservoir

(diameter, 1.5 mm) located near the inlet facilitates visualization of the filling process (Fig. S2). The capabilities for performing measurements of concentrations of creatinine and urea in sweat along with sweat dynamics in a single platform provide a technical foundation for future studies of the relationships between these concentrations and sweat rate.

### Sweat induction and collection

Collection of sweat can be accomplished via initiation based on physical exercise, mental stress, exposure to warm, humid environments (e.g. a saunas) or delivery of stimulating agonists to the sweat glands with electrical current.<sup>9,36-38</sup> The first two methods have utility in certain contexts, but they do not apply effectively to infants or to elderly patients, nor can they be used more generally with subjects whose health conditions prevents exercise. The third requires access to specialized facilities. The

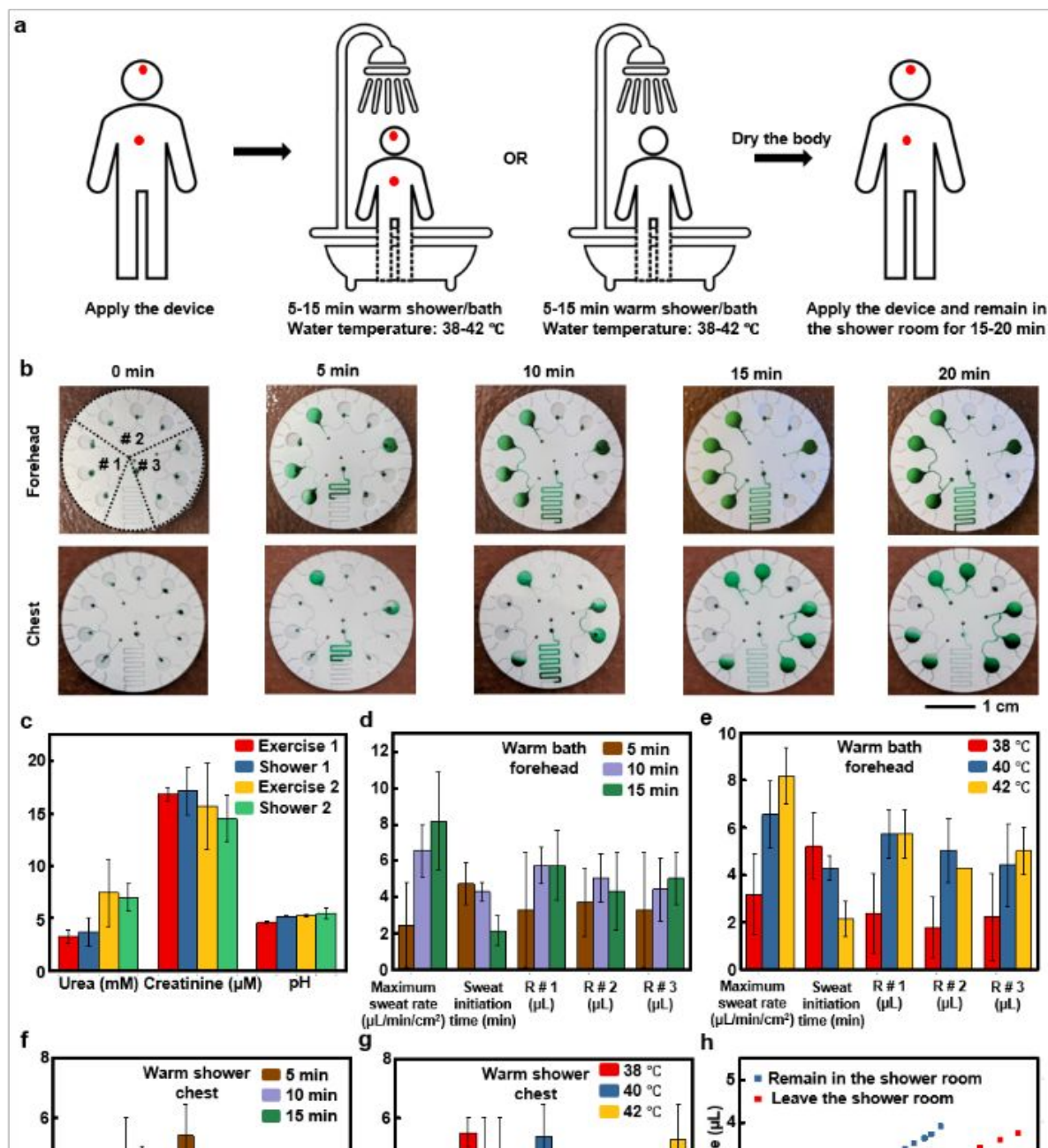


**Figure 3.** Sweat induction and collection during and/or after warm-water showering/bathing. (a) Schematic illustration of procedures to collect sweat using a skin-interfaced microfluidic device during and/or after warm-water showering/bathing. (b) Representative optical images of epidermal microfluidic devices spotted with green dye at the inlets of  $\mu$ -channels and  $\mu$ -reservoirs to aid in visualizing the collection of sweat during/after warm-water showering. (c) Data that illustrate that the shower/bath environment does not dilute the concentrations of sweat creatinine, urea, and its pH. (d-g) Maximum sweat rate, time to start the sweat, and the collected sweat volumes in  $\mu$ -reservoirs for various collection conditions. (h) Comparison of collected sweat volumes for remaining inside the shower room and moving outside the room after the shower.

sweat rate initiation (μL) (μL) (μL) sweat rate initiation (μL) (μL) (μL) time (min)

(μL/min/cm<sup>2</sup>) time (min) (μL/min/cm<sup>2</sup>) time (min)

fourth also demands special setups, and the process can also induce pain and/or inflammation at the skin interface. Here we introduce a patient-friendly, convenient method that can be applied in the home. The process captures sweat immediately after or during warm-water showering or bathing, as illustrated schematically in Fig. 3a. Fig. 3b presents representative optical images of devices for sweat captured after emerging from a shower, applied on the forehead and chest after drying with a towel and cleaning with an alcohol pad. Fig. 3b suggests that this method can capture several microliters of sweat easily from these locations even with the unoptimized designs reported here ( $\sim 0.18 \text{ cm}^2$  collection zone) within 15 min, for on-demand collection and *in situ* analysis. Experimental studies suggest that there are no significant differences between the concentrations of urea or creatinine, or of pH in sweat captured in this manner compared to that obtained via physical exercise, for comparable rates (Fig. 3c, Table S1).

Experiments at three different water temperatures (38, 40, and 42 °C) for three different durations (5, 10 and 15 min) at

begins within a few minutes. Increasing the temperature of the water from 38 to 42 °C and the length of the shower and bath from 5 to 15 min, reduces the initiation time and increases the sweat rate, respectively. Experimental results for other conditions including shower/forehead and bath/chest show similar trends, as in Figs. 3 and S3. Only minor differences in sweat generation profiles occur for collection times of 10 and 15 min and for water temperatures of 40 °C and 42 °C, for both bathing and showering. The relative humidity level in the shower room stabilizes around 99% for various conditions. The temperature of the room is an important factor. As shown in Fig. 3h, collection in the bathing/shower room ( $\sim 28 \text{ °C}$ ) leads to a constant sweat rate. Collection outside of this room (20 °C, relative humidity level 70-80%) leads to decreases in the sweat rate, as might be expected. For bathing, sweat capture occurs more efficiently from the forehead than the chest (Figs. 3 and S3), consistent with the high density of sweat glands on the former.<sup>64</sup> Interestingly, for the warm-water shower, the chest yields more sweat than the forehead (Figs. 3 and S3), possibly

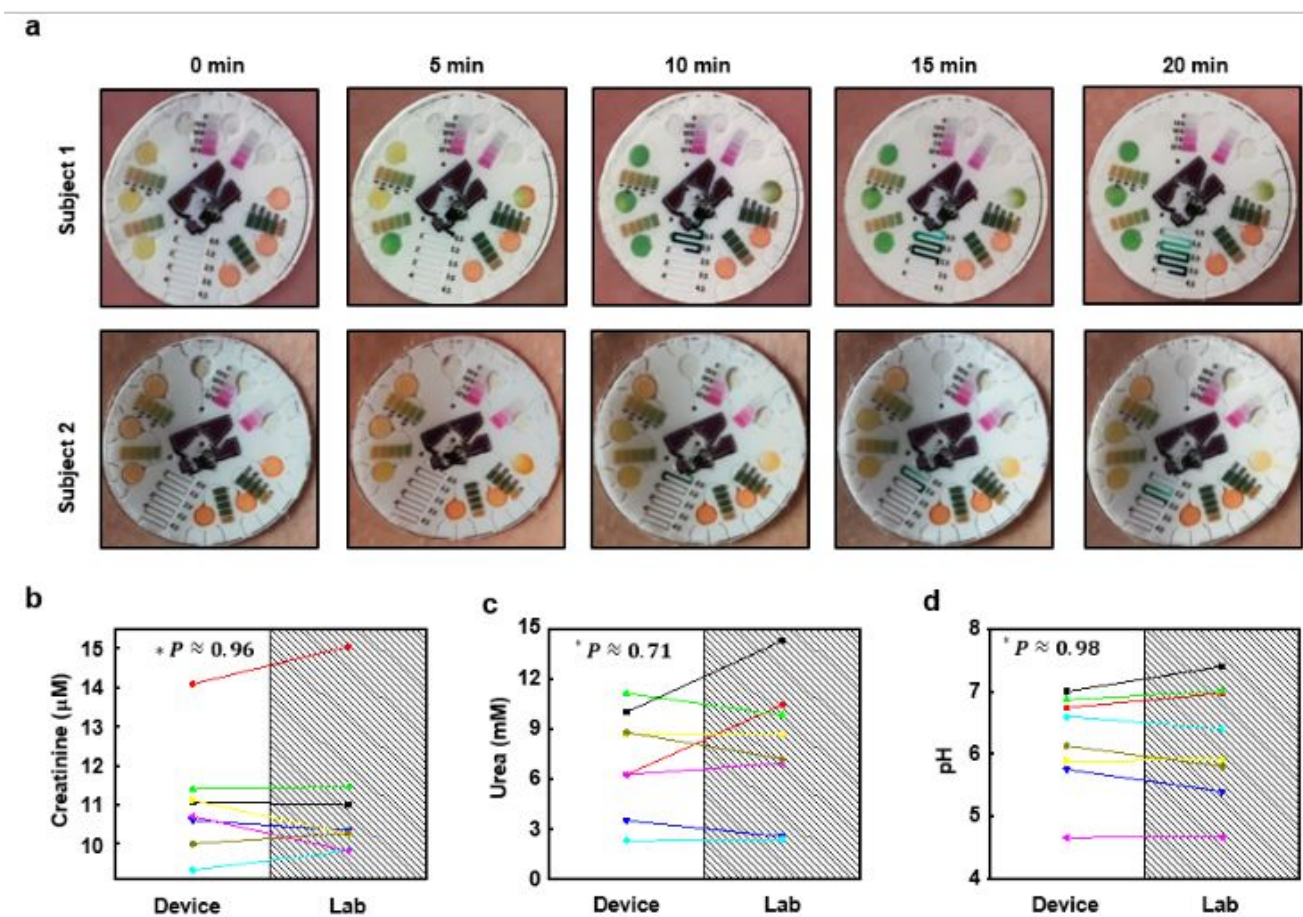


**Figure 4.** Human subject studies. (a) Images of devices applied to the forehead and chest collected at various times during the study. (b), (c), and (d) Concentrations of biomarkers in sweat obtained using the devices versus laboratory-based analysis of sweat collected from absorbing pads ( $n=8$ ). Data points with the same color are measured during the same test. \*  $P < 0.05$ , two-tailed test.

two body locations (forehead and chest) provide additional insights into the process. As illustrated in the shower/chest and bath/forehead study in Figs. 3d-g and Table S2, sweat collection

due to the local warming effect of clothing on the former.

Further adaptations of the devices simplify the process by allowing for sweat collection during the showering/bathing

session itself. Figs. S4a and b show devices that feature a capillary bursting at the outlet to prevent backfilling of water in these cases.<sup>40,65</sup> Other modifications include a reduction of the volumes of the  $\mu$ -reservoirs from 2.2  $\mu$ L to 1.0  $\mu$ L. With this reduced capacity, the serpentine channel, added after the  $\mu$ -reservoir, fills with sweat after the  $\mu$ -reservoir, thereby preventing dye or chemicals in the  $\mu$ -reservoir from passing directly onto the skin. Figs. S4c-d demonstrate that sweat can be captured in this manner (showering with water temperature of 40 °C; duration: 10 min). Experimental observations suggest that a negligible amount of water passes from the bath/shower through the constituent materials of the devices and into the channels/ $\mu$ -reservoirs during the collection period, consistent with approximate diffusion calculations. Observations also suggest that no backfilling occurs.

### Field studies

The studies use epidermal microfluidic devices mounted on the forehead and chest of healthy volunteers, with sweat capture immediately after exiting the shower in the shower room. This process fills the  $\mu$ -reservoirs with sweat to allow assessments via colorimetric measurements of digital images. Sweat enters the device and fills each  $\mu$ -reservoir in a sequential fashion. Sweat does not continue to enter a  $\mu$ -reservoir that is already full. This configuration avoids dilution and flow-through effects that might otherwise alter the color development. In practical testing, color extraction only occurs from filled  $\mu$ -reservoirs. Specifically, capturing an image of the device using a smartphone camera yields data that can be used to determine concentrations of creatinine and urea, and pH (Fig. 4a). In parallel, conventional collection methods using absorbent pads taped to the skin and covered with films of polyimide (25  $\mu$ m thick) to prevent sweat evaporation yield  $\sim$ 1 mL volume of sweat from the forehead for subsequent instrumental analysis using LC-MS/MS, NMR, and a pH meter (Fig. S5). As shown in Figs. 4b-d and Fig. S6, creatinine and urea concentrations and pH values measured using the microfluidic skin-interfaced devices exhibit good correlation to those determined using standard approaches. The results for different subjects range from 9  $\mu$ M to 15  $\mu$ M for creatinine, 2 mM to 15 mM for urea, and 4.5-7.5 for pH, all of which are consistent with normal values for healthy subjects.<sup>16,23,39</sup> In addition to digital image analysis, the color reference markers facilitate approximate analysis by simple visual inspection, possibly of use in rapid disease screening.

### Conclusions

The findings presented here establish the utility of a user-friendly, convenient method for sweat capture and analysis that uses soft, skin-interfaced microfluidic devices and natural sweat processes that occur during and/or immediately after warm-water showering or bathing. A collection of enzymatic chemistries enables colorimetric sensing of creatinine and urea in sweat, and a standard indicator yields pH values, each of potential relevance for diagnosing and/or monitoring patients

with kidney disease. Studies of human subjects demonstrate these capabilities, with validation against standard collection schemes and laboratory diagnostic instruments.

## Materials and methods

### Device fabrication

Patterning photoresist (KMPR 1010; Microchem, MA, USA) on a silicon wafer (1 mm thick) and deep reactive ion etching (STS Pegasus ICP-DRIE; SPTS Technologies, Newport, United Kingdom) of the exposed regions generated a pattern of relief in the geometry of the  $\mu$ -channels and  $\mu$ -reservoirs. A thin layer of poly(methylmethacrylate) (PMMA; Microchem, MA, USA) spin cast (3000 rpm) onto this silicon mold to serve as an anti-adhesion layer. Pouring a mixture of a white dye (Reynolds Advanced Material, 5% wt) and a precursor of PDMS (Sylgard 184 at a 10:1 mixing ratio of base to curing agent; Dow Corning, MI, USA) on the mold, spin coating at 200 rpm and baking at 70 °C for 45 min generated the microfluidic channel layer ( $\sim$ 550  $\mu$ m thick). The chemical assays were located at the positions of the  $\mu$ -reservoirs. Separately, sequential spin coating of precursors of PDMS with mixing ratios of 10:1 and 50:1 at 400 and 1000 rpm, respectively, for 1 min and then baking at 70 °C for 45 min yielded a capping layer ( $\sim$ 350  $\mu$ m thick). The 50:1 PDMS provided a tacky surface to facilitate bonding to the microfluidic channel layer. A transparent polyester film (25  $\mu$ m thick; THERMLfilm SELECT® 10852; FLEXcon, MA, USA) placed on top of the device supported the color reference markers. A corona treatment (30 s; Electro-Technic Products) enabled bonding of a medical grade acrylate adhesive (60  $\mu$ m thick; 1524; 3M, MN, USA) the bottom of the device for robust adhesion to the skin.

### Forming the colorimetric assays

- 1) Urea: A 0.01 mg/mL solution of urease (urease from *Canavalia ensiformis*, Jack bean, type III; Sigma-Aldrich, MO, USA) was prepared in deionized water (pH=7). Immobilizing 2  $\mu$ L of this solution onto piece of pH paper (diameter, 3 mm, Hydrion Strips B 1-11, Micro Essential Laboratory, NY, USA) and drying under vacuum in a desiccator for 15 min yielded the assay.
- 2) Creatinine: Mixing creatininase, creatinase, and enzyme in a 1:1:1 ratio yielded the creatinine assay solution. Spotting 0.5  $\mu$ L of this cocktail solution onto the  $\mu$ -reservoir and drying under vacuum in a desiccator for 1 h produced the assay. Next, spotting 0.25  $\mu$ L of creatinine probe at an adjacent location and drying in a desiccator for another 1 h completed the process. (Creatinine Assay Kit; Sigma-Aldrich, MO, USA).
- 3) pH: pH cocktail solution resulted from thoroughly vortexing 4 mL of universal pH dye (Fisher Scientific, NH, USA), 274 mg of polyvinyl chloride (M.W.  $\sim$ 233,000, Sigma-Aldrich, MO, USA), 635  $\mu$ L of o-nitrophenyloctylether (Sigma-Aldrich, MO, USA) and 508  $\mu$ L of aliquot in 10 mL of tetrahydrofuran (Sigma-Aldrich, MO, USA) to yield a homogenous suspension. Dipping a piece of filter paper into the resulting solution for 10 s and allowing it to dry under ambient conditions for 15 min formed a solid-state pH assay. Finally, a metal punch (diameter, 3 mm)

cut circular pads of the paper to sizes to match those of the  $\mu$ -reservoirs.

#### Standard color development and color reference marker preparation

Color reference markers facilitate accurate color extraction under a range of illumination conditions. Preparation of these markers began with in vitro tests using standard samples of artificial sweat to produce reference colors. Digital imaging and analysis under controlled lighting provided color value for each assay. Standard solutions of creatinine use commercial materials (Sigma-Aldrich, MO, USA) and artificial sweat. Those for urea (Sigma-Aldrich, MO, USA) used artificial sweat for urea. The pH buffer solution used artificial sweat for creatinine with pH adjusted with NaOH (Sigma-Aldrich, MO, USA). A pH meter (Mettler Toledo, Greifensee, Switzerland) determined the pH value. The tests for creatinine, urea and pH each used 2  $\mu$ L of standard solution in the  $\mu$ -reservoirs. Here, the volume of 2  $\mu$ L was selected to match the size of  $\mu$ -reservoirs in the microfluidic system. Incubation involved heating in an oven at 37 °C for 15 min. A digital SLR camera (EOS 6D; Canon, Tokyo, Japan) captured the images. Photoshop (Adobe Systems, CA, USA) served as a means for extracting color information. The white background of the microfluidic device established reference for white balance. A color laser printer (C454 PS; Konica Minolta, Tokyo, Japan) produced a reference marker on PET film at 1200 DPI resolution, with colors to match those determined using the methods described above.

#### Laboratory analysis of creatinine, urea, and pH

**NMR.** All  $^1\text{H}$  NMR experiments were performed on a Bruker Neo 600 MHz system equipped with a z-gradient HFCN Cryo probe. A series of standard urea solutions ranging from 1 mM to 500 mM was prepared by dissolving 0.3003 g urea crystal in 5 mL artificial sweat and diluting with artificial sweat. Samples of sweat were passed through syringe filters with pore size 0.2  $\mu$ m (Sigma-Aldrich, MO, USA). Each sample was mixed with 5%  $\text{D}_2\text{O}$  (v/v) and 500  $\mu$ L volumes of each were loaded into a standard 5 mm NMR tube for the measurements. Urea and water signals were measured following a reported sequence.<sup>49</sup> The receiver gain was fixed at 25.4 for all sample. For different samples, the free induction decay (FID) signal was set from 1-64 for a decent signal to noise ratio. Each sample was analyzed 3 times.

**LC-MS/MS.** The method for determining creatinine with LC-MS/MS appears elsewhere.<sup>66</sup> Chromatographic separation of creatinine and creatinine-d3 were performed on an Atlantis Silica HILIC 3  $\mu$ m 2.1 mm x 50 mm column (Waters, MA, USA). The flow rate was maintained at 0.3 mL/min. The gradient was 5% A for 1 min, to 55% A in 6 min, at 55% A for 2 min, to 5% A in 0.1 min, at 5% A for 1.9 min, where A was water with 0.1% formic acid and B was acetonitrile with 0.1% formic acid. Quantification of creatinine was performed on a Bruker AmaZon-X. Creatinine and creatinine-d3 were monitored using characteristic precursor-production ion transitions: 114->86 for creatinine and 117->89 for creatinine-d3. Creatinine-d3 served as an internal standard solution. The calibration standard

solution of creatinine (Sigma-Aldrich, MO, USA) ranging from 1 to 1000  $\mu$ M was prepared with 1% formic acid. The internal standard solution of creatinine-d3 (CDN Isotopes, Quebec, Canada) was finalized at 500  $\mu$ M in 1% formic acid. Sweat samples were also filtered before measurement. Each sample was mixed with the internal standard solution in a 5:1 ratio. The concentration of creatinine was calculated from the peak area ratio of creatinine to creatinine-d3. Each sample was analyzed 3 times.

**pH.** Analysis of sweat pH was conducted with a pocket ion sensitive field effect transistor (ISFET) pH meter (Model 24004, DeltaTrak, CA, USA), which required only 50  $\mu$ L of sweat sample.

**Human testing.** Testing involved healthy young adults as volunteers during normal physical activity with no additional human-subject risk. All subjects provided their consent prior to participation.

For comparisons between sweat induced by showering and exercising, each volunteer engaged in 30 min of exercise and 10 min of shower at 40 °C. The sweat for laboratory analysis was collected with a Kimwipe (Fisher Scientific, NH, USA) covered with a 25  $\mu$ m thick film of polyimide to prevent evaporation or moisture condensation during exercise and shower. Each sweat sample was centrifuged and filtered before analysis.

For studies of sweat induction and collection, the water temperature was adjusted to the testing temperature (38, 40, or 42 °C) with subjects then engaging in a shower/ bath for a well-defined time duration (5, 10, or 15 min). To study the effect of time duration, the testing temperature was controlled at 40 °C. To study the effect of temperature, time duration was controlled at 5 min for shower and 10 min for bath. Sweat collection devices were attached onto desired locations where they remained in place for 15-20 min after exiting the shower/bath or before shower/bath depending on the device and experimental design. Images were collected to record the volume at different times for calculations of sweat rate and total volume.

For field studies, subjects engaged in a warm shower at 40 °C for 10 min as described previously, followed by attachment of devices on desired body locations. After 15 to 40 min, digital images were collected using a smartphone for further image analysis. White balance was performed with reference to the white microfluidic channel. Analysis at three different locations from each assay provided an averaged color value that was then matched to the average value for the corresponding reference marker to yield concentrations for each biomarker. Most colorimetric results correspond to evaluations from a single filled  $\mu$ -reservoir. In cases with multiple filled  $\mu$ -reservoirs, the colors were the same, to within uncertainties.

#### Calculations of diffusive transport

The water may diffuse through the device and into the  $\mu$ -channels during the shower/bath. Here, a one-dimensional model for diffusion of water into the film is established. The polyester layer serves as the main barrier to prevent diffusion of water into the devices or sweat out of the devices. The diffusivity of water in polyester is at least three orders of

magnitude lower than that in PDMS.<sup>67,68</sup> Here, we only consider diffusion in polyester. With the origin located at the bottom and the  $y$  axis in thickness direction running upward, the diffusion equation is

$$D \frac{\partial^2 w}{\partial y^2} = \frac{\partial w}{\partial t}, 0 \leq y \leq h_0 \quad (1)$$

where  $w$  is the water concentration that depends on position  $y$  and time  $t$ ,  $D$  the water diffusivity in polyester, and  $h_0$  the initial thicknesses of the polyester layer. A constant water concentration  $w_0$  at the top surface and zero water concentration at the bottom surface of the polyester layer give the boundary conditions

$$\begin{aligned} w|_{y=h_0} &= w_0 \\ w|_{y=0} &= 0 \end{aligned} \quad (2)$$

The initial condition of zero water concentration in polyester gives

$$w|_{t=0} = 0 \quad (0 \leq y < h_0) \quad (3)$$

By the method of separation of variables,

$$w = Y(y)T(t) \quad (4)$$

which yields

$$D \frac{Y''}{Y} = \frac{T'}{T} = -\lambda \quad (5)$$

with  $\lambda$  being the eigenvalue. By solving Eq. (5), we have

$$\begin{aligned} Y &= E \sin\left(\sqrt{\frac{\lambda}{D}}y\right) + F \cos\left(\sqrt{\frac{\lambda}{D}}y\right) \\ T &= e^{-\lambda t} \end{aligned} \quad (6)$$

where  $E$  and  $F$  are constants to be determined. According the homogeneous boundary conditions of Eq. (2), i.e.,  $w|_{y=h_0} = 0$  and  $w|_{y=0} = 0$ , we have  $Y|_{y=h_0} = 0$  and  $Y|_{y=0} = 0$ , which give  $F = 0$  and

$$\sin\left(\sqrt{\frac{\lambda}{D}}h_0\right) = 0 \quad (7)$$

The eigenvalues are thus obtained from Eq. (7) as

$$\lambda_n = D \left(\frac{n\pi}{h_0}\right)^2 \quad (n=1,2,3,\dots) \quad (8)$$

Therefore, the homogeneous solution of water concentration is

$$w_h = \sum_{n=1}^{\infty} \left[ C_n e^{-D \left(\frac{n\pi}{h_0}\right)^2 t} \sin\left(\frac{n\pi}{h_0}y\right) \right] \quad (9)$$

with the constants  $C_n$  to be determined. The general solution of the problem is obtained by the sum of Eq. (9) and a particular solution  $w_p = w_0 y/h_0$  that satisfies Eqs. (1) and (2):

$$w = \frac{w_0}{h_0}y + \sum_{n=1}^{\infty} \left[ C_n e^{-D \left(\frac{n\pi}{h_0}\right)^2 t} \sin\left(\frac{n\pi}{h_0}y\right) \right] \quad (10)$$

Substituting Eq. (10) into the initial condition in Eq. (3), we obtain

$$C_n = \frac{2(-1)^n w_0}{n\pi} \quad (11)$$

The final solution is thus obtained as

$$w(y,t) = w_0 \left\{ \frac{y}{h_0} + \sum_{n=1}^{\infty} \frac{2(-1)^n}{n\pi} e^{-D \left(\frac{n\pi}{h_0}\right)^2 t} \sin\left(\frac{n\pi}{h_0}y\right) \right\} \quad (12)$$

The water volume through the polyester layer within the time period  $0 - \Delta t$  is determined by  $v_{\text{water}} = \int_0^{\Delta t} D \partial w / \partial y|_{y=0} A dt / w_0$ , where  $A$  represents the cross-sectional area of the  $\mu$ -reservoir. Further simplification gives

$$v_{\text{water}} = \frac{D\pi r^2}{h_0} \int_0^{\Delta t} \theta\left(\frac{1}{2}; \frac{D\pi t}{h_0^2}\right) dt \quad (13)$$

where  $r$  is the radius of the  $\mu$ -reservoir, and  $\theta(z; \tau) = 1 + 2 \sum_{n=1}^{\infty} e^{i\pi n^2 \tau} \cos(2\pi n z)$  is the Jacobi theta function, where  $i$  is the imaginary unit. With  $D \times 10^{12} = 0.025 - 0.78 \text{ m}^2 \text{ s}^{-1}$  (at  $90^\circ \text{C}$ ),<sup>68</sup>  $r = 1.1 \text{ mm}$ ,  $h_0 = 25 \text{ }\mu\text{m}$ , and  $\Delta t = 20 \text{ min}$ , the amount of water that passes is  $2 \times 10^{-5} - 0.13 \text{ }\mu\text{L}$ .

## Conflicts of interest

J.A.R. and R.G. co-founded a company, Epicore Biosystems, Inc., which develops soft microfluidics systems for commercial deployment.

## Acknowledgements

Y. Z., H. G., S. B. K. contributed equally to this work. Y.Z. acknowledges financial support from the University of Missouri - Columbia start - up fund. R.L. acknowledges the support from the Young Elite Scientists Sponsorship Program by CAST (grant 2015QNRC001) and Fundamental Research Funds for the Central Universities (grant DUT18GF101). This work utilized Northwestern University Micro/Nano Fabrication Facility (NUFAB), which is partially supported by Soft and Hybrid Nanotechnology Experimental (SHyNE) Resource (NSF ECCS-1542205). This work made use of the Integrated Molecular Structure Education and Research Center (IMSERC) at Northwestern, which is partially supported by NIH 1S10OD012016-01/1S10RR019071-01A1 and the Office for Research at Northwestern University.

## Additional information

Electronic supplementary file is available.

Fig. S1. The dynamics of urease-urea hydrolysis reaction in different pH conditions.

Fig. S2. Demonstration of sweat rate measurement.

Fig. S3. Sweat collection study under bath/chest (top) and shower/forehead (bottom).

Fig. S4. A microfluidic design to enables sweat collection during shower/bath.

Fig. S5. Traditional methods for urea and creatinine determination.

Fig. S6. Statistical analysis of the concentration of biomarkers obtained from device results and laboratory results.

Table S1. Statistical analysis of different sweat induction methods as shown in Fig. 3c.

Table S2. Statistical analysis of different shower/bath conditions as shown in Figs. 3d-g

Fig. S1 demonstrates the urease-urea hydrolysis reaction dynamics at different pH conditions. Figs. S1a-c show color development and the corresponding normalized percentage change of the red level with time at various sweat pH.

Fig. S2 demonstrates the method for determining the sweat rate using the serpentine microfluidic channel. The volume and time were recorded to allow extraction of the average sweat rate from the slope (Figs. S2a-b). Figs. S2c-d show schematic illustrations and pictures of the setup, which consists of a pressure generator, a pressure controller, and a fluidic container.

Studies of sweat induction and collection used experimental results at two locations (forehead and chest) under each condition.

The results from shower/forehead and bath/chest are shown in Fig. S3. Sweat rate increases and the initiation time decreases with increasing water temperature and duration of the shower/bath. The sweat rate and sweat volume for the cases of shower/forehead and bath/chest are smaller than the corresponding values for the shower/chest and bath/forehead. Field tests were performed under conditions to yield large sweat rate and volume.

Fig. S4 shows a modified microfluidic design (Figs. S4a-b) with a small  $\mu$ -reservoir volume (1  $\mu$ L) and a capillary bursting valve (Fig. S4b) at the outlet to prevent water from flowing into the channel. Figs. S4c-d compare sweat of this design and the previous one for use on the forehead and chest during a warm shower (water temperature: 40 °C, duration: 10 min), where the end time for showering is the reference time. According to Fig. S4c, sweating can be initiated during and after shower. The modified device has enhanced capability for capturing sweat during shower.

Fig. S5 shows laboratory analysis of creatinine and urea using LC-MS/MS and NMR. The extracted ion chromatogram of characteristic precursor-production ion transitions for creatinine (114->86) and creatinine-d3 (117->89) are demonstrated in Fig. S5a. <sup>1</sup>H NMR spectra for urea detection are shown in Fig. S5b, with water suppression for the left spectrum and normal sequence for the right spectrum. The linear fitting

of standard laboratory analysis of urea and creatinine are shown Fig. S5c-d.

Fig. S6 demonstrates a statistical analysis of the correlation of creatinine and urea concentration, and of pH determined using the microfluidic devices and laboratory instrumentation. The linear fitting of device and laboratory results yield a slope around 1 and a good correlation coefficient ( $R^2 > 0.6$ ).

Table S1 shows statistical analysis of different sweat induction methods.

Table S2 shows statistical analysis of different shower/bath conditions.

## Notes and references

1. J. Choi, R. Ghaffari, L. B. Baker and J. A. Rogers, *Sci. Adv.*, 2018, **4**.
2. M. Bariya, H. Y. Y. Nyein and A. Javey, *Nat. Electron.*, 2018, **1**, 160-171.
3. A. Mena-Bravo and M. D. L. de Castro, *J. Pharm. Biomed. Anal.*, 2014, **90**, 139-147.
4. J. K. Davis, L. B. Baker, K. Barnes, C. Ungaro and J. Stofan, *Sports Med.*, 2016, **46**, 1391-1405.
5. P. M. Farrell, B. J. Rosenstein, T. B. White, F. J. Accurso, C. Castellani, G. R. Cutting, P. R. Durie, V. A. LeGrys, J. Massie, R. B. Parad, M. J. Rock and P. W. Campbell, *J. Pediatr.*, 2008, **153**, S4-S14.
6. H. Lee, C. Song, Y. S. Hong, M. S. Kim, H. R. Cho, T. Kang, K. Shin, S. H. Choi, T. Hyeon and D. H. Kim, *Sci. Adv.*, 2017, **3**.
7. A. Kaushik, A. Vasudev, S. K. Arya, S. K. Pasha and S. Bhansali, *Biosens. Bioelectron.*, 2014, **53**, 499-512.
8. O. Parlak, S. T. Keene, A. Marais, V. F. Curto and A. Salleo, *Sci. Adv.*, 2018, **4**.
9. S. Emaminejad, W. Gao, E. Wu, Z. A. Davies, H. Y. Y. Nyein, S. Challa, S. P. Ryan, H. M. Fahad, K. Chen, Z. Shahpar, S. Talebi, C. Milla, A. Javey and R. W. Davis, *Proc. Natl. Acad. Sci. U. S. A.*, 2017, **114**, 4625-4630.
10. J. T. Korpelainen, K. A. Sotaniemi and V. V. Myllyla, *Stroke*, 1992, **23**, 1271-1275.
11. H. Y. Y. Nyein, L. C. Tai, Q. P. Ngo, M. H. Chao, G. B. Zhang, W. Gao, M. Bariya, J. Bullock, H. Kim, H. M. Fahad and A. Javey, *ACS Sens.*, 2018, **3**, 944-952.
12. Z. Sonner, E. Wilder, J. Heikenfeld, G. Kasting, F. Beyette, D. Swaile, F. Sherman, J. Joyce, J. Hagen, N. Kelley-Loughnane and R. Naik, *Biomicrofluidics*, 2015, **9**.
13. S. B. Kim, K. Lee, M. S. Raj, B. Lee, J. T. Reeder, J. Koo, A. Hourlier-Fargette, A. J. Bandodkar, S. M. Won, Y. Sekine, J. Choi, Y. Zhang, J. Yoon, B. H. Kim, Y. Yun, S. Lee, J. Shin, J. Kim, R. Ghaffari and J. A. Rogers, *Small*, 2018, **14**.
14. H. M. Emrich, E. Stoll, B. Friolet, J. P. Colombo, R. Richterich and E. Rossi, *Pediatr. Res.*, 1968, **2**, 464-478.
15. M. J. Buono, K. D. Ball and F. W. Kolkhorst, *J. Appl. Physiol.*, 2007, **103**, 990-994.
16. C. T. Huang, M. L. Chen, L. L. Huang and I. F. Mao, *Chin. J. Physiol.*, 2002, **45**, 109-115.
17. A. S. Levey, J. P. Bosch, J. B. Lewis, T. Greene, N. Rogers and D. Roth, *Ann. Intern. Med.*, 1999, **130**, 461-470.
18. D. J. van Veldhuisen, L. M. Ruilope, A. S. Maisel and K. Damman, *Eur. Heart J.*, 2016, **37**, 2577-U2513.
19. J. P. Kassirer, *N. Engl. J. Med.*, 1971, **285**, 385-389.
20. U. Lad, S. Khokhar and G. M. Kale, *Anal. Chem.*, 2008, **80**, 7910-7917.

21. A. Tricoli and G. Neri, *Sensors*, 2018, **18**.
22. R. W. Keller, J. L. Bailey, Y. H. Wang, J. D. Klein and J. M. Sands, *Physiol. Rep.*, 2016, **4**.
23. Y. Y. AlTamer, E. A. Hadi and I. E. I. AlBadrani, *Urol. Res.*, 1997, **25**, 337-340.
24. T. C. Boysen, S. Yanagawa, F. Sato and K. Sato, *J. Appl. Physiol.: Respir., Environ. Exercise Physiol.*, 1984, **56**, 1302-1307.
25. V. F. Curto, C. Fay, S. Coyle, R. Byrne, C. O'Toole, C. Barry, S. Hughes, N. Moyna, D. Diamond and F. Benito-Lopez, *Sens. Actuators, B*, 2012, **171**, 1327-1334.
26. M. J. Patterson, S. D. R. Galloway and M. A. Nimmo, *Acta Physiol. Scand.*, 2002, **174**, 41-46.
27. R. M. Morgan, M. J. Patterson and M. A. Nimmo, *Acta Physiol. Scand.*, 2004, **182**, 37-43.
28. N. Nakanishi, M. Fukui, M. Tanaka, H. Toda, S. Imai, M. Yamazaki, G. Hasegawa, Y. Oda and N. Nakamura, *Kidney Blood Pressure Res.*, 2012, **35**, 77-81.
29. E. Gallardo and J. A. Queiroz, *Biomed. Chromatogr.*, 2008, **22**, 795-821.
30. W. Gao, S. Emaminejad, H. Y. Y. Nyein, S. Challa, K. V. Chen, A. Peck, H. M. Fahad, H. Ota, H. Shiraki, D. Kiriya, D. H. Lien, G. A. Brooks, R. W. Davis and A. Javey, *Nature*, 2016, **529**, 509-+.
31. A. J. Bandodkar and J. Wang, *Trends Biotechnol.*, 2014, **32**, 363-371.
32. D. H. Kim, N. S. Lu, R. Ma, Y. S. Kim, R. H. Kim, S. D. Wang, J. Wu, S. M. Won, H. Tao, A. Islam, K. J. Yu, T. I. Kim, R. Chowdhury, M. Ying, L. Z. Xu, M. Li, H. J. Chung, H. Keum, M. McCormick, P. Liu, Y. W. Zhang, F. G. Omenetto, Y. G. Huang, T. Coleman and J. A. Rogers, *Science*, 2011, **333**, 838-843.
33. J. Kim, A. Banks, H. Y. Cheng, Z. Q. Xie, S. Xu, K. I. Jang, J. W. Lee, Z. J. Liu, P. Gutruf, X. Huang, P. H. Wei, F. Liu, K. Li, M. Dalal, R. Ghaffari, X. Feng, Y. G. Huang, S. Gupta, U. Paik and J. A. Rogers, *Small*, 2015, **11**, 906-912.
34. J. D. Pegan, J. Zhang, M. Chu, T. Nguyen, S. J. Park, A. Paul, J. Kim, M. Bachman and M. Khine, *Nanoscale*, 2016, **8**, 17295-17303.
35. T. Yokota, P. Zalar, M. Kaltenbrunner, H. Jinno, N. Matsuhisa, H. Kitanosako, Y. Tachibana, W. Yukita, M. Koizumi and T. Someya, *Sci. Adv.*, 2016, **2**.
36. S. B. Kim, Y. Zhang, S. M. Won, A. J. Bandodkar, Y. Sekine, Y. G. Xue, J. Koo, S. W. Harshman, J. A. Martin, J. M. Park, T. R. Ray, K. E. Crawford, K. T. Lee, J. Choi, R. L. Pitsch, C. C. Grigsby, A. J. Strang, Y. Y. Chen, S. Xu, J. Kim, A. Koh, J. S. Ha, Y. G. Huang, S. W. Kim and J. A. Rogers, *Small*, 2018, **14**.
37. Y. Sekine, S. B. Kim, Y. Zhang, A. J. Bandodkar, S. Xu, J. Choi, M. Irie, T. R. Ray, P. Kohli, N. Kozai, T. Sugita, Y. X. Wu, K. Lee, K. T. Lee, R. Ghaffari and J. A. Rogers, *Lab Chip*, 2018, **18**, 2178-2186.
38. A. Hoshi, H. Watanabe, M. Kobayashi, M. Chiba, Y. Inaba, N. Kimura and T. Ito, *Tohoku J. Exp. Med.*, 2001, **195**, 163-169.
39. A. Koh, D. Kang, Y. Xue, S. Lee, R. M. Pielak, J. Kim, T. Hwang, S. Min, A. Banks, P. Bastien, M. C. Manco, L. Wang, K. R. Ammann, K. I. Jang, P. Won, S. Han, R. Ghaffari, U. Paik, M. J. Slepian, G. Balooch, Y. G. Huang and J. A. Rogers, *Sci. Transl. Med.*, 2016, **8**.
40. J. Choi, D. Kang, S. Han, S. B. Kim and J. A. Rogers, *Adv. Healthcare Mater.*, 2017, **6**.
41. M. Jaffé, *Zeitschrift für physiologische Chemie*, 1886, **10**, 391-400.
42. M. J. Welch, A. Cohen, H. S. Hertz, K. J. Ng, R. Schaffer, P. Van der Lijn and E. t. White, *Anal. Chem.*, 1986, **58**, 1681-1685.
43. D. Tsikas, A. Wolf, A. Mitschke, F. M. Gutzki, W. Will and M. Bader, *J. Chromatogr. B: Anal. Technol. Biomed. Life Sci.*, 2010, **878**, 2582-2592.
44. J. A. Muñoz, M. López-Mesas and M. Valiente, *Talanta*, 2010, **81**, 392-397.
45. H. Crocker, M. D. Shephard and G. H. White, *J. Clin. Pathol.*, 1988, **41**, 576-581.
46. T. K. With, *Acta Physiol. Scand.*, 1945, **10**, 355-365.
47. J. S. Wang, Y. Gao, D. W. Dorshorst, F. Cai, M. Bremer, D. Milanowski, T. L. Staton, S. S. Cape, B. Dean and X. Ding, *J. Pharm. Biomed. Anal.*, 2017, **133**, 96-104.
48. M. Czauderna and J. Kowalczyk, *Czech J. Anim. Sci.*, 2012, **57**, 19-27.
49. L. Liu, H. Mo, S. Wei and D. Raftery, *Analyst*, 2012, **137**, 595-600.
50. Y. P. Chen, B. Liu, H. T. Lian and X. Y. Sun, *Electroanalysis*, 2011, **23**, 1454-1461.
51. W. O. Ho, S. Krause, C. J. McNeil, J. A. Pritchard, R. D. Armstrong, D. Athey and K. Rawson, *Anal. Chem.*, 1999, **71**, 1940-1946.
52. R. Sha, K. Komori and S. Badhulika, *Electrochim. Acta*, 2017, **233**, 44-51.
53. J. L. Orsonneau, C. Massoubre, M. Cabanes and P. Lustenberger, *Clin. Chem.*, 1992, **38**, 619-623.
54. Z. F. Gao, E. E. Sann, X. D. Lou, R. Y. Liu, J. Dai, X. L. Zuo, F. Xia and L. Jiang, *NPG Asia Mater.*, 2018, **10**, 177-189.
55. L. Li, Y. Long, J. M. Gao, K. Song and G. Q. Yang, *Nanoscale*, 2016, **8**, 4458-4462.
56. P. T. Vasdudevan and Y. Gokarn, *Appl. Biochem. Biotechnol.*, 1996, **60**, 49-61.
57. J. Kim, T. N. Cho, G. Valdes-Ramirez and J. Wang, *Talanta*, 2016, **150**, 622-628.
58. M. Fidaleo and R. Lavecchia, *Chem. Biochem. Eng. Q.*, 2003, **17**, 311-318.
59. H. Lee, T. K. Choi, Y. B. Lee, H. R. Cho, R. Ghaffari, L. Wang, H. J. Choi, T. D. Chung, N. S. Lu, T. Hyeon, S. H. Choi and D. H. Kim, *Nat. Nanotechnol.*, 2016, **11**, 566-+.
60. M. Pearcy, S. Robinson, D. I. Miller, J. T. Thomas, Jr. and J. Debrot, *J. Appl. Physiol.*, 1956, **8**, 621-626.
61. W. F. Clark, J. M. Sontrop, S. H. Huang, L. Moist, N. Bouby and L. Bankir, *Am. J. Nephrol.*, 2016, **43**, 281-292.
62. P. Salvo, F. Di Francesco, D. Costanzo, C. Ferrari, M. G. Trivella and D. De Rossi, *IEEE Sens. J.*, 2010, **10**, 1557-1558.
63. S. Coyle, D. Morris, K. Lau, D. Diamond, N. Taccini, D. Costanzo, P. Salvo, F. D. Francesco, M. G. Trivella, J. Porchet and J. Luprano, 2009.
64. N. A. Taylor and C. A. Machado-Moreira, *Extrem. Physiol. Med.*, 2013, **2**, 4.
65. H. Cho, H. Y. Kim, J. Y. Kang and T. S. Kim, *J. Colloid Interface Sci.*, 2007, **306**, 379-385.
66. X. Q. Zhao, S. H. Zeisel and S. C. Zhang, *Electrophoresis*, 2015, **36**, 2207-2214.
67. G. C. Randall and P. S. Doyle, *Proc. Natl. Acad. Sci. U. S. A.*, 2005, **102**, 10813-10818.
68. N. L. Post, F. Riebel, A. Zhou, T. Keller, S. W. Case and J. J. Lesko, *J. Compos. Mater.*, 2009, **43**, 75-96.